Microstructured BN composites with internally designed high thermal conductivity paths for 3D electronic packaging

*Hongying He, Weixiang Peng, Junbo Liu, Xin Ying Chan, Shike Liu, Li Lu, Hortense Le Ferrand**

Dr. H. He, Dr. W. Peng, J. Liu, X. Y. Chan, Dr. H. Le Ferrand
School of Mechanical and Aerospace Engineering
Nanyang Technological University
50 Nanyang Avenue, 639798, Singapore
Email: hortense@ntu.edu.sg

S. Liu, Dr. H. Le Ferrand
School of Materials Science and Engineering
Nanyang Technological University
50 Nanyang Avenue, 639798, Singapore

Prof. L. Lu
Department of Mechanical Engineering
National University of Singapore
9 Engineering Drive 1, 117575, Singapore
National University of Singapore (Chongqing) Research Institute, 401123, China

Keywords
boron nitride composites, high thermal conductivity, platelet orientation, microstructure design, directional heat dissipation

Miniaturized and high-power density 3D electronic devices pose new challenges on thermal management. Indeed, prompt heat dissipation in electrically insulating packaging is currently limited by the thermal conductivity achieved by thermal interface materials (TIMs) and by their capability to direct the heat towards heat sinks. Here, we create high thermal conductivity BN-based composites able to conduct heat intentionally towards specific areas by locally orienting magnetically functionalized BN microplatelets using magnetically assisted slip casting (MASC). The obtained thermal conductivity along the direction of alignment is unusually high, up to 12.1 W m^{-1} K^{-1} thanks to a high concentration of 62.6 vol% of BN in the composite, a low

concentration in polymeric binder and a high degree of alignment. The BN composites have a low density of 1.3 g cm^{-3}, a high stiffness of 442.3 MPa and are electrically insulating. Uniquely, we demonstrate our approach with proof-of-concept composites having locally graded orientations of BN microplatelets to direct the heat away from two vertically stacked heat sources. Rationally designing the microstructure of TIMs to direct heat strategically provides a promising solution for efficient thermal management in 3D integrated electronics.

1. Introduction

The rapid development of miniaturized, high power density, and integrated electronic devices challenges current heat dissipation management.[1-4] To guarantee the lifespan and reliability of electronic devices, the heat generated by the electronic components is traditionally conducted to a heat sink via a thermal interface material (TIM) that has a high thermal conductivity.[5-7] In three-dimensional (3D) electronics of high packing density where electronic chips are stacked into multilayers or 3D matrices, conventional TIMs may pose a problem of local overheating by channeling the heat between the stacked electronics.[8] A proposed approach to enhance heat dissipation in such complex assemblies is to intentionally direct the heat into specific directions. To date, numerous examples of TIMs with directional heat transfer have been obtained using aligned graphitic or metallic anisotropic fillers.[9] However, the use of electrically conductive materials is a problem in high power density electronics due to electric arc issues. Furthermore, the direction of heat transfer has mostly been studied through the thickness of the TIMs which would be a problem in vertical stacks of electronic chips. There is thus a need to achieve electrically insulating but highly thermally conductive TIMs with tunable and local directions of heat transfer.

TIMs made from hexagonal boron nitride (BN) are promising to obtain electrically insulation and high thermal conductivity thanks to the excellent in-plane thermal conductivity $K_{\parallel}$ ~ 400 W m^{-1} K^{-1} of individual BN microplatelets, whereas their through-plane thermal conductivity $K_{\perp}$ is only about 30 W m^{-1} K^{-1} due to the phonon scattering among the stacked BN nanosheets, leading to the highly anisotropic thermal conductive properties.[10-13] Furthermore, directionality in the thermal conduction can be achieved by aligning the BN parallel to each other. Various methods have been used to orient BN platelets for anisotropic thermal conduction, such as tape casting,[11,14] vacuum-assisted filtration,[15] hot pressing,[16] shear-induced 3D printing,[17] freeze casting,[18-19] coating on structured substrate,[51-52] and magnetic fields. [20-22] Compared to the other methods, magnetic alignment provides the advantage of precisely and remotely controlling the local orientation of anisotropic platelets.

Also, any orientation angle can easily be programmed by simply changing the magnetic field direction. Indeed, contrary to the other methods that realized horizontal orientations, magnetic fields have been able to create vertically aligned BN composites. This has been typically achieved by coating the platelets with iron oxide and applying a low magnetic field, below 50 mT, to a liquid composite mixture before its consolidation by curing. Thanks to the vertical alignment, the thermal conductivity through the thickness of the materials has been greatly increased. For example, vertically aligned BN-epoxy composites containing 20 wt% BN showed a thermal conductivity of 0.85 W m^{-1} K^{-1} along the vertical direction, which is twice more than in random configurations.[20] Similarly, BN-silicone composites with 9.14 vol% BN platelets oriented parallel and perpendicular to the heat flux exhibited 44.5% higher and 37.9% lower thermal conductivity than the unaligned composites, respectively.[21] More recently, Gurijala et al. reported improved through-thickness thermal conductivity of 8.67 W m^{-1} K^{-1} in BN-polymer composites by vertically aligning BN microplatelets at a solid loading of 60 vol%.[22] However, more complex microstructures have not been yet realized and explored for their application in 3D chips assemblies.

Complex microstructures in highly concentrated microplatelet assemblies can be realized using a method called magnetically assisted slip casting (MASC).[23] During MASC, a liquid slurry composed of magnetically responsive particles suspended in a low viscosity solvent is cast onto a porous substrate under a low magnetic field. As the solvent gets removed through the pores of the substrate, the concentration in particles increases, leading to the consolidation of the structure and the locking of their orientation. Using MASC and varying the magnetic field orientation in a step-wise manner, multilayer structures with multiple and purposely designed local orientations have been realized in composites containing 40 vol% or more alumina microplatelets.[24-26] Using MASC with BN microplatelets instead of alumina could therefore achieve high BN concentration and programmed local orientation. The high concentration in BN microplatelets and the low polymer concentration in the composites obtained after MASC could induce close contacts between the particles, reducing their interfacial resistance and increasing the overall thermal conductivity. At the same time, the alignment of the microplatelets parallel to each other would further increase the contact area between percolating particles and the direction of alignment of their basal plane bestowing high conductivity $K_{\parallel}$ could form an “express highway” to channel the heat.

Herein, we therefore used MASC to produce BN-PVP composites with complex microstructures intentionally designed to channel the heat effectively into specific directions. To achieve such composites, the optimum concentration in BN microplatelets to use in the

slurry to attain high orientational control is first determined using rheology and electron microscopy. Then, this optimum slurry, which is found to contain 40 wt% BN microplatelets, is used to create purposely oriented microstructures. The thermal properties of the composites are then characterized and related to the quality and direction of alignment, with vertically oriented samples reaching an outstanding through-thickness thermal conductivity of 12.1 W m^{-1} K^{-1} that is higher than other values reported to date. The mechanical and electrical properties of the composites with various orientations are also tested to help envision their realistic application. Finally, composites with complex microstructures are produced as proof-of-concept examples of directional thermal transport to specific directions for efficient thermal management in 3D electronic chip assemblies. The experimental results are supported by finite element simulations and illustrate the capability of microstructure design. The results provided in this research open new possibilities for high power density electronic devices.

2. Results and Discussion

To use MASC to produce oriented BN composites, it is first necessary to determine the optimum slurry composition to simultaneously achieve high BN concentration and high BN alignment (**Figure 1**). **Figure 1a** summarizes the preparation of the microstructure-controlled BN-PVP composites. As raw crystalline BN microplatelets (average lateral size 45 μm, **Figure S1a**, Supplementary Information (SI)) are not intrinsically magnetic and do not align under low magnetic fields (< 1 T), they are first rendered magnetically responsive by electrostatically adsorbing cationic superparamagnetic iron oxide nanoparticles (SPIONs) on their surface (**Figure 1b,c**; **Figure S1c**). Then, the functionalized BN microplatelets (m-BN) are suspended in an aqueous slurry in presence of a small concentration of polyvinyl pyrrolidone (PVP) to act as a binder. During casting of the slurry onto the porous gypsum, a low magnetic field rotating at about 1 Hz is applied to orient the m-BN. After complete drying, the final composite is readily obtained without further need for high-temperature treatment, crosslinking, or curing. This fabrication approach hallmarks several merits. i) Fabrication of lightweight materials (**Figure 1d)**: the composites obtained have a density of 1.3 g cm^{-3} independently of the solid loading in the slurry. Lightweight materials are advantageous as they avoid heavy loading of the thermal management material onto electronic devices. Also, this density corresponds to about 62.6 vol% in BN which is a high solid concentration promising for obtaining high thermal conductivity. ii) Free dimension: the casted composites can be bulk with controlled thickness, where the shapes and dimensions can be further customized and upscaled. iii) Environmentally friendly

process: MASC avoids the use of harsh chemicals or high energy consuming procedures, enabling more sustainable products.

Besides these qualities, MASC produces highly oriented microstructures if the solid loading in the slurry is adequate.[25] Indeed, under the application of the rotating magnetic field, the m-BN microplatelets undergo dynamic movements in response to magnetic, viscous, and gravitational torques before settling into the preferential direction set by the magnet.[25] Given the need for the microplatelets to rotate and orient themselves, the viscosity of the slurry plays the pivotal role. This viscosity is directly tailored by the concentration in microplatelets and should be neither too high that the microplatelets cannot rotate, nor too low that their orientation will collapse after drying. In addition, changing the molecular weight of PVP polymer will also affect the viscosity, where the amount of polymer should be adjusted accordingly to provide proper slurry viscosity. Measurement of the viscosity for slurries containing 20 to 50 wt% m-BN shows the expected increase (**Figure 1e**). Compared to a slurry made of alumina microplatelets, our viscosities are one order of magnitude lower, suggesting that magnetic orientation should happen.[24] To verify that the m-BN retain their orientation after drying, BN-PVP composites were prepared under a vertical magnetic field using slurries with different solid loadings. After MASC, all the composites exhibited the expected densely packed and highly oriented microstructures with vertical microplatelets (**Figure 1f)**. The quality of the orientation could be quantified using the conformation factor C_f defined as:

$$C_f = \frac{F_M}{F_N} \qquad (1)$$

where F_M and F_N are the full width at half maximum (FWHM) of the gray value curve along the major and minor axis, respectively, of the ellipse of the fast Fourier transform (FFT) fitted with a Gaussian function (see SI for details and **Figure S2**). The higher the C_f , the higher the degree of alignment. According to **Figure 1f**, an optimum C_f value of 4.5 was obtained for the slurry concentration of 40 wt%. This result was confirmed using X-ray diffraction (XRD) analysis of the composite cross sections (**Figure 1g**), which contain the side edges of the vertically oriented BN microplatelets. The degree of orientation δ as the evaluation of overall BN microplatelets alignment level is defined as:

$$\delta = \frac{I_{100}}{I_{002} + I_{100}} \times 100\% \qquad (2)$$

where I_{100} is the intensity of the (100) peak corresponding to the vertical orientation, and I_{002} is the intensity of the (002) peak corresponding to the horizontal orientation.[21,27] For the composite made from the slurry containing 40 wt% m-BN, δ attained the highest value of 90%

confirming the high orientation. Microstructured BN-PVP composites can therefore be prepared using MASC from an aqueous slurry containing 40 wt% of the m-BN. The next section will discuss the rational design of controlling the microplatelets alignment direction to induce high thermal conductivity in the composites.

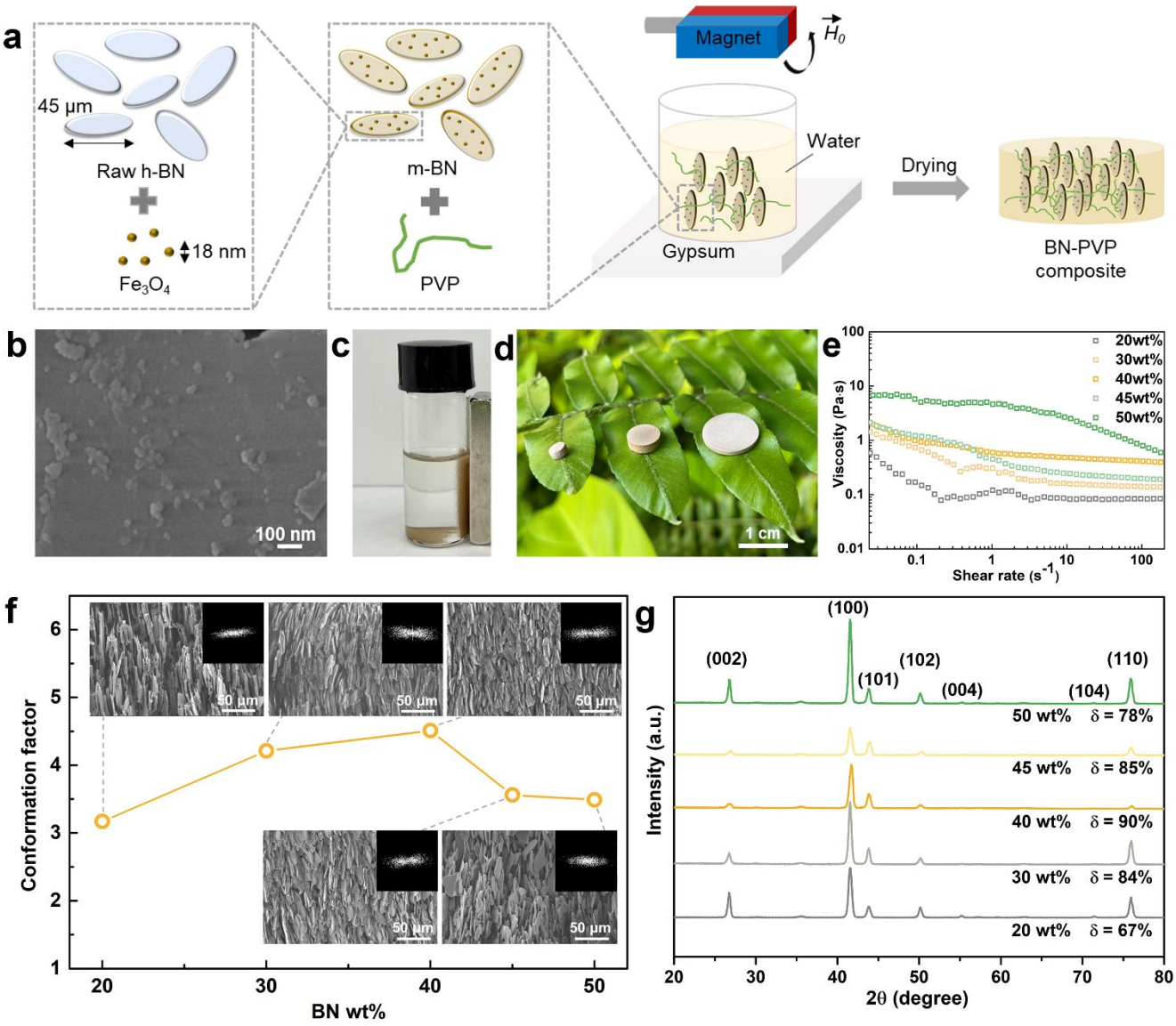

Figure 1. a) Schematics of the composite fabrication: magnetization of BN microplatelets (m-BN), preparation of BN-PVP slurries, and orientation of m-BN using MASC to produce aligned composites. b) Micrograph of the surface of a m-BN microplatelet showing the coating with iron oxide nanoparticles. c) Picture showing m-BN powder dispersed in ethanol being attracted to a permanent magnet. d) Picture of BN-PVP composites of various dimensions placed onto plant's leaves, illustrating their low weight. e) Viscosity of the BN-PVP aqueous slurries as a function of the shear rate at concentrations in m-BN from 20 to 50 wt%. f) Conformation factor C_f of BN-PVP composites prepared under vertical orientation as a function of m-BN concentration in the slurry and corresponding cross-sectional micrographs of the composites and their Fast-Fourier Transform (FFT) patterns (inserts). g) XRD patterns of the vertically aligned composites for increasing m-BN content in the slurry and the corresponding degree of orientation δ.

After MASC, the BN-PVP composites contain high concentration in BN particles that form a percolating network, as well as high alignment. The microplatelet alignment and orientation will not only induce directionality in the thermal conduction but also facilitate the thermal transport by alleviating the thermal resistance between adjacent microplatelets. Indeed, thermal transport in ceramics relies on phonon propagation which are crystal lattice vibrations. Ideally, the lattice vibrations between percolating particles should therefore be coupled, which is the case for aligned microplatelets. Engineering the direction of orientation of the BN microplatelets therefore has the double benefit of increasing the thermal conductivity by creating high phonon mean free paths and directing the phonon transport along specific planes (**Figure 2a-c**). In random configurations, the disordered arrangement with varying contact angles between adjacent microplatelets leads to reduced interplatelet contact area (**Figure 2a**). Phonons traveling from a heat source placed underneath the randomly oriented composite would therefore be scattered in all directions, diffusing the heat in the composite. At the same time, the thermal transport between adjacent microplatelets will be impeded by the reduced contact area and increased interfacial resistance. Contrary to randomly oriented composites, aligned composites have larger contact areas between adjacent microplatelets, reducing the interfacial resistance and facilitating phonon transfer from one microplatelet to the other. Also, microplatelets alignment concentrates the phonon transport within the plane of alignment, creating an "express highway" path for phonons to travel. Therefore, horizontally aligned composites would find their maximum thermal conductivity along their horizontal plane. Hence, the heat from a source placed underneath the composite would be spread in the horizontal plane towards the sides of the composite, leading to low through-thickness thermal conduction (**Figure 2b**). In contrast, composites with vertically aligned BN microplatelets will have their direction of maximum thermal conductivity along vertical planes. Therefore, the heat from a source placed underneath the composite would be efficiently channeled to the top surface where a heat sink could be placed to further cool down the material, for example (**Figure 2c**). Furthermore, since the high thermal conductivity is along a 2D surface, the heat will also be efficiently channeled towards the edges of the composites, increasing the overall surface area available to cool the composite. Adequately, our experimental fabrication method allows the fabrication of the three microstructures discussed (**Figure 2d-f**). The conformation factors C_f of 4.5 and 4.4 for the vertically and horizontally aligned composites, respectively, indicate the similarly high alignment quality, whereas the unaligned, random composite had an expected low C_f of 1.1. The alignment quality was also confirmed using XRD as well as visual color inspection (**Figures S3** and **S4**, SI). Understanding the relationship between the microplatelet

orientation and the thermal transport “express highways” is needed for rationally designing next-generation TIMs. Indeed, conventional TIMs connect a heat source, typically an electronic chip, with a heat sink (**Figure 2g**). In this case, high thermal conductivity through the thickness of the TIM composites is required. However, in other cases for example in high power density electronic devices where chips are stacked in 3D assemblies, the heat generated from one electronic chip cannot be simply channeled vertically as it would encounter other electrical components. It would therefore be desirable to have a TIM that channels the heat towards selected directions. Thanks to MASC, it is possible to create gradients of microplatelets orientations to turn the direction of high thermal conductivity while maintaining a high contact area between aligned microplatelets (**Figure 2h**). These two examples of “traditional” TIMs with high through-thickness thermal conductivity and “next-generation” TIMs with directed heat transport are experimentally characterized in the following and compared with other existing BN composites.

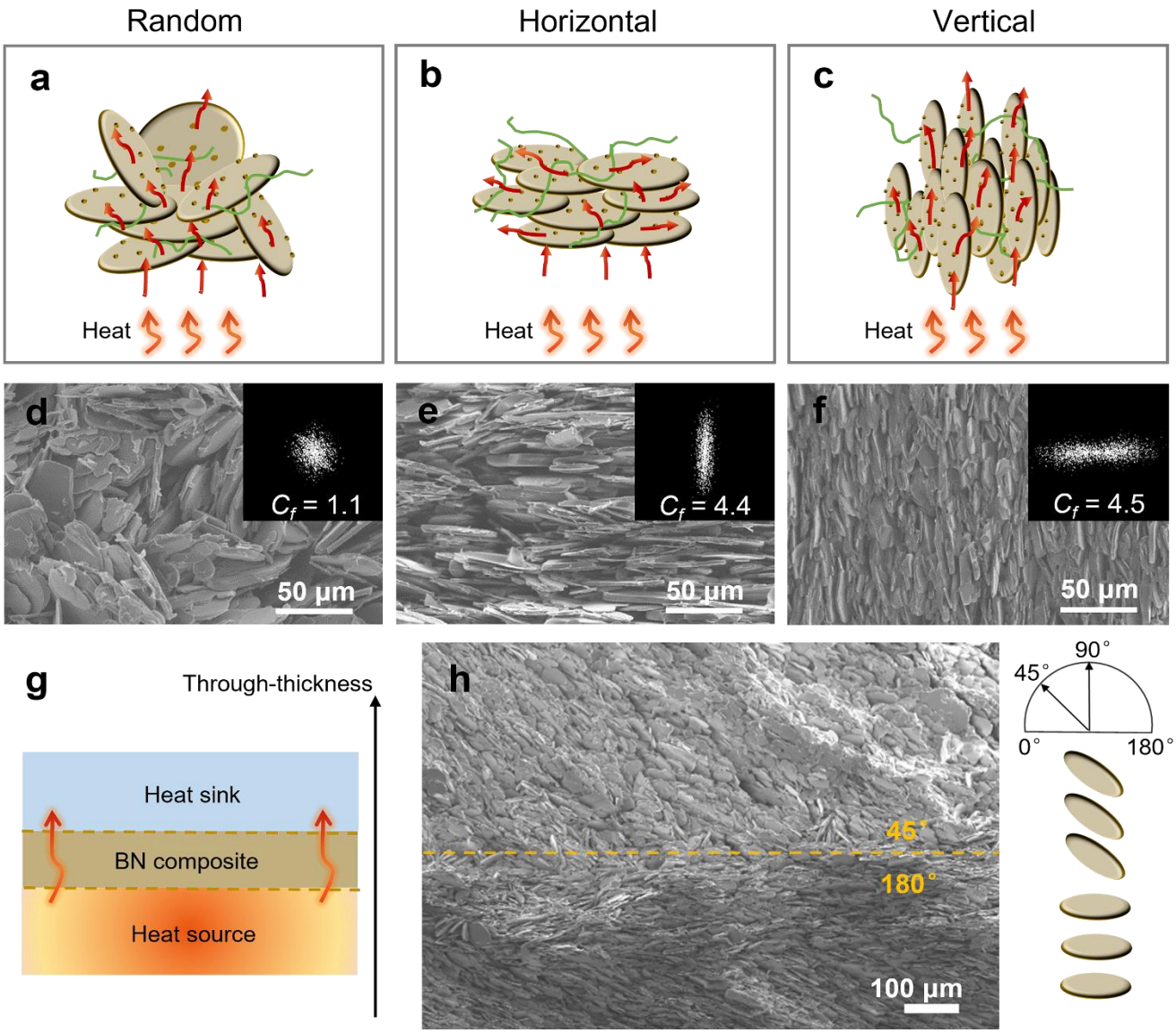

Figure 2. Schematic illustration of heat transport paths in a) randomly, b) horizontally, and c) vertically aligned BN-PVP composites prepared using MASC. The heat transfer paths are indicated with red arrows. Electron micrographs and corresponding FFT patterns and conformation factor C_f of cross sections of the BN-PVP composites prepared with a slurry containing 40 wt% m-BN and with d) random, e) horizontal, and f) vertical alignment. g) Schematic of the application of BN composite as thermal interface material. h) Electron micrograph of the cross section of a BN-PVP composite with a graded microplatelet orientation at angles from 45° to 180°.

For "traditional" TIM applications, we found that our BN-PVP composites exhibited superior performance as compared to other BN composites in the literature (**Figure 3)**. We explain these results by the high alignment quality obtained with our fabrication approach. Indeed, after MASC, all composites exhibited the similar solid loading in BN of about 60 vol%, yet the composites prepared using 40 wt% BN yielded the highest C_f. It is therefore expected that vertically aligned composites resulting from this slurry would yield the highest through-thickness thermal conductivity. This is what was measured experimentally with an unusually high conductivity of 12.1 W m^{-1} K^{-1}, which is about 6 times higher than that obtained with a

slurry containing 20 wt% m-BN (**Figure 3a)**. Although the similarly high degree of orientation were observed from the composites using 30 wt% (δ = 84%) and 45 wt% (δ = 85%) m-BN (**Figure 1g**), the 45 wt% composition exhibited the higher thermal conductivity due to the formation of percolating networks at a higher filler concentration. Furthermore, using the optimum slurry containing 40 wt% m-BN, the direction of orientation also has the anticipated drastic effect on the through-thickness thermal conductivity with a large increase from 0.6 W m^{-1} K^{-1} for horizontally aligned composites, to a 20-fold increase achieved in the vertical ones (**Figure 3b**). Interestingly, the randomly aligned composites have a conductivity of 1.7 W m^{-1} K^{-1} which is higher than for the horizontal ones. This is likely due to the very high thermal conductivity within the in-plane direction of the horizontal composite. Indeed, aligned microstructure assemblies exaggerate the anisotropic thermal conductive nature of BN microplatelets compared with random structures. In the horizontally aligned composites, nearly all platelets are oriented horizontally and the contribution to the thermal conduction through the thickness of the composite is limited. The through-plane thermal conductivity of BN microplatelets is only about 30 W m^{-1} K^{-1} due to the pronounced phonon scattering among the stacked BN nanosheet layers. Therefore, the thermal conduction through the thickness of the composites is suppressed in horizontally aligned composites, which is even lower than that in random alignment. In addition to the ultra-high thermal conductivity in the vertically aligned samples, excellent thermal stability was also recorded (**Figure 3c**). The high thermal conductivity was maintained up to 200 °C and after several heating and cooling cycles, suggesting that the composites fulfill the working conditions required for electronic applications. Although PVP is hygroscopic in nature and has a glass transition temperature of about 180 °C, the composites are stable up to 350 °C (**Figure S5**, SI). Despite the poor intrinsic thermal conductivity of PVP (~ 0.1 W m^{-1} K^{-1}),[28] our vertically-aligned BN-PVP composites possessed a superior through-thickness thermal conductivity as compared to the literature, including BN nanosheet (BNNS) composites whose reported values are typically below 5 W m^{-1} K^{-1} (**Figure 3d** and **Table S1**, SI).[20-22,29-49]

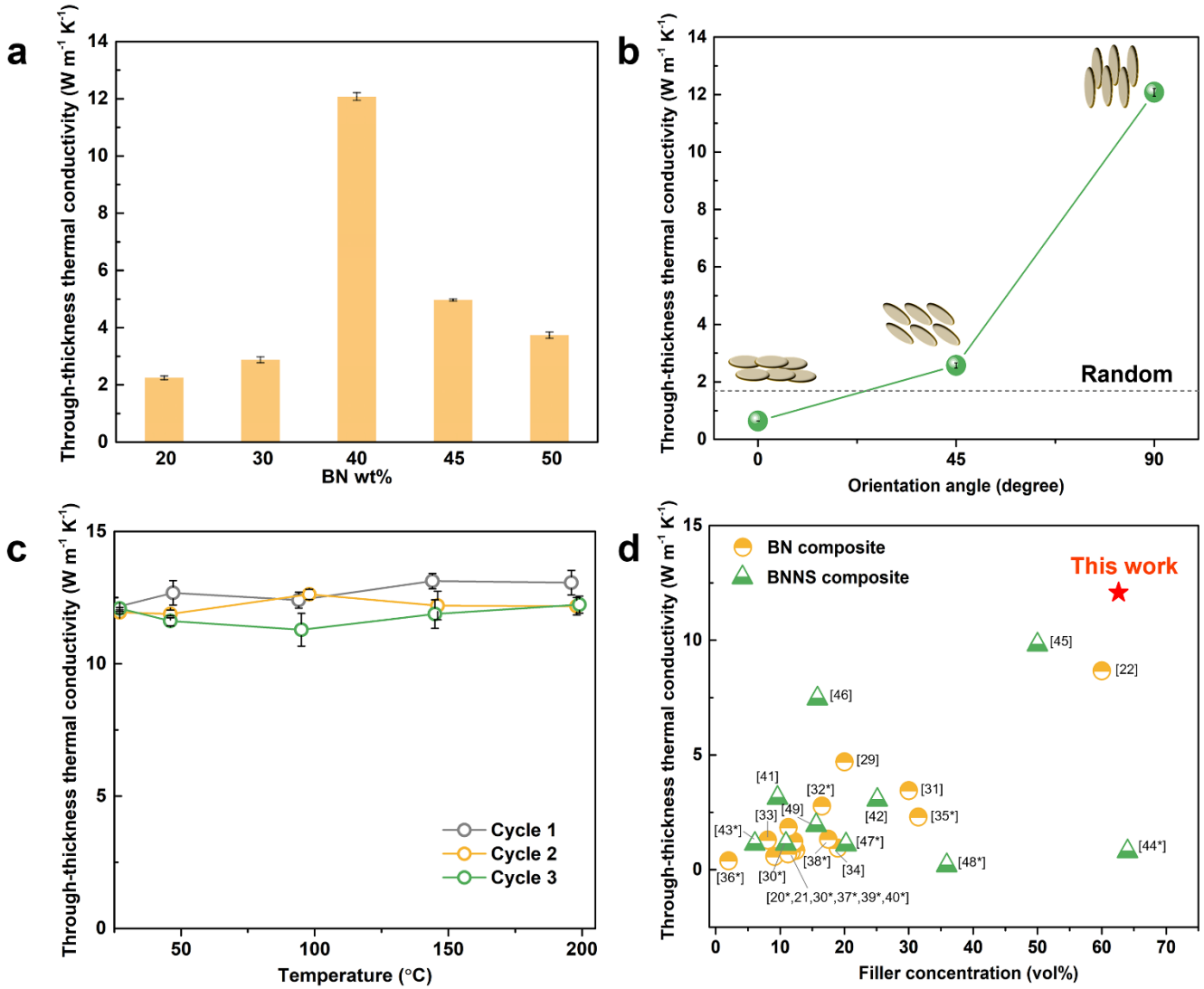

Figure 3. a) Through-thickness thermal conductivity of BN-PVP composites prepared under vertically rotating magnetic fields as a function of BN concentration used in the slurry. b) Through-thickness thermal conductivity of BN-PVP composites prepared using the slurry containing 40 wt% BN, as a function of their orientation angle of 0°, 45°, to 90° and compared with the randomly aligned composites. c) Through-thickness thermal stability of BN-PVP composites with vertical alignment and prepared from the 40 wt% slurry, in the temperature range from 25 to 200 °C for 3 repetitive heating-cooling cycles. d) Comparison of the through-thickness thermal conductivity of this work with other various BN composites reported in the literature. The results are also compared to exfoliated BNNS-based composites. The volume concentration of the data points in references labelled with asterisk symbol were estimated and converted from wt% to vol% by using the reported density of fillers and matrix.

This outstanding performance can be attributed to the following factors. First, the large lateral size of the BN microplatelets of 45 μm used in this study provides lower interfacial thermal resistance thanks to the large contact area between neighboring platelets. Also, larger platelets reduce the amount of platelet boundaries and interfaces as compared to composites containing smaller platelets. Second, the BN microplatelets were highly crystalline and used without exfoliation. This preserves their stiffness and their lattice structures without inducing corrugated structures or local crystal defects, facilitating the phonon transport. Third, the

composite fabrication process yields simultaneously a high concentration in BN filler of 62.6 vol%, together with the precise orientation control. Fourth, the low concentration in polymer and iron oxide nanoparticles likely further reduces the interfacial resistance between percolating particles facilitating phonon transport. Finally, the high orientation level alleviates the phonon scattering from the misalignment of adjacent particles so that the phonon heat transportation can be unidirectional and continuous along the alignment direction, leading to an outstanding thermal diffusivity of 14.1 $mm^2 s^{-1}$ (**Table S2**, SI). The high filler loading, homogenous filler distribution, and closely packed microstructure guarantee the formation of an interconnected network, allowing the construction of the "express highway" for continuous phonon transport.

The outstanding performance of our vertically aligned MASCed BN-PVP composites shows the advantage of the method to produce "traditional" TIMs with high through-thickness thermal dissipation. Also, controlling the microstructure in composites with high relative densities permits to attain adequate mechanical performance for electronic applications. Before proceeding with demonstration of complex microstructured TIMs for 3D electronics, we further verify that the mechanical and electrical properties of the composites would support high energy power density and mechanical loading (**Figure 4**). Tested under compression at room temperature, the composites exhibited the expected behavior with vertically aligned BN possessing a modulus of 442.3 MPa and a strength of 2.0 MPa exceeding those of the composites with horizontal and random alignment (**Figure 4a**). Surprisingly, the Vickers hardness of vertically aligned composites was lower than those with random alignment but was higher than the horizontally aligned ones (**Figure 4b**). This could be due to the higher spread of the load in random composites than in the vertical ones. In turn, the moderate hardness in vertically aligned composites could facilitate the physical contact with electronic components during assembly. These results show that in addition to the thermal conductivity, designing the microstructure of the composites could be exploited to tune their mechanical properties to produce more reliable and resistant TIMs. In addition, slightly different thermal expansion characteristics could be expected in various oriented microstructures. **Figure 4c** shows similarly high electrical resistivities of the BN-PVP composites with different BN orientations, suggesting their electrical insulating property which is an important characteristic in high power density electronics. Moreover, the frequency dependence of their dielectric properties at room temperature are shown in **Figure 4d.** A low dielectric constant of TIMs composites is generally preferred to avoid failure of the electronic device due to electromagnetic interference. Here, at the frequency of 1 kHz, the vertical, horizontal, and random composites exhibited low dielectric constants of 4.9, 2.8, and 3.6, respectively, and only slightly increased upon decreasing

frequency, ensuring low signal distortion in application. Interestingly, the vertically aligned composite exhibited relatively higher dielectric constant and more obvious frequency dependence of the dielectric constant, especially at the lower frequency range, than the horizontally and randomly oriented composites. The higher dielectric constant in the vertically aligned sample suggests the more pronounced charge build-up when the microplatelets orientation is in the same direction as the applied electric field, and also reflects the anisotropic dielectric properties of single BN microplatelets.[53]

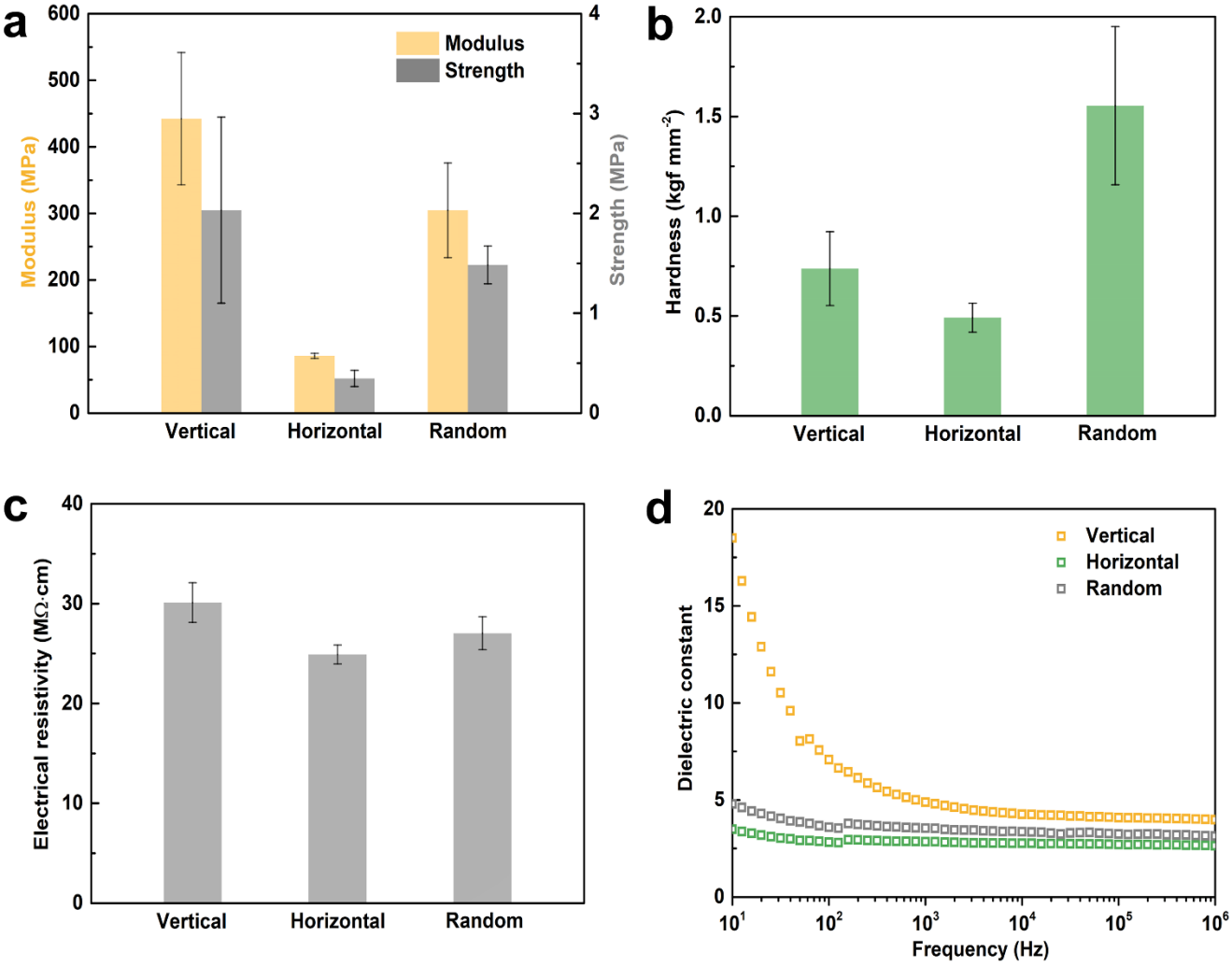

Figure 4. Mechanical and electrical properties of BN-PVP composites prepared using the slurry containing 40 wt% m-BN and with vertical, horizontal, and random orientations: a) compression modulus and strength, b) Vickers hardness, c) electrical resistivity, and d) dielectric constant at room temperature in the frequency range of 10 Hz to 1 MHz.

Having demonstrated that microstructure design can enhance the performance of BN-PVP composites for "traditional" TIM applications, we now discuss and experimentally test unusual microstructures in our BN-PVP composites to illustrate how the design capability allowed by

the simple fabrication method using MASC can be leveraged for more complex applications in 3D electronics. Specifically, we produce proof-of-concept composites with graded microstructures that channel the heat away from two heat sources sandwiching the composite. Using MASC, we produced BN-PVP composites with selected microstructures to demonstrate the capability to control highly thermal conductive pathways in unusual and as-designed directions. Specifically, gradients in BN orientations within the microstructures were tested in view of their applications to channel the heat generated by two opposing heat sources. The fabricated composites were tested in heating and cooling operations to evaluate how fast they can transport heat as well as the local heat distribution in the microstructures (**Figure 5**). First, we prepared composites with a single orientational gradient and tested them with the horizontal side in contact with the heat source (case H→V) and with the vertical side in contact with the heat source (case V→H) and compared their response with purely horizontal (H) and vertical (V) orientations (**Figure 5a-f**).

In the first set of experiments, we placed the composites on a hot substrate heated to ~100 °C and recorded the increase in temperature of the top surface using an infrared camera (**Figure 5a**, **Figure S6)**. The substrate was left to cool down naturally. All the microstructured composites heated up after contact with the hot substrate, with the vertically oriented ones heating fastest. Interestingly, a "heating band" across the central axis of the vertically aligned composites is clearly observed due to the anisotropy of the BN microplatelets. This confirms the earlier discussion that not only the heat conduction is fast through the thickness of the samples, but also that there is a high thermal conductive path along the alignment direction in the plane (**Figure 2c**). After 10 s, the vertically aligned composites reached their highest surface temperature and the temperature recorded started to decrease because the substrate was cooling down. The vertically aligned composites exhibited the fastest surface temperature increase, with an increase from 30 to 50 °C in less than 5 s (**Figure 5b)**. Given the thickness of 1.5 mm of the composites, the initial speed of the temperature increase was about 4 °C s^{-1}, which is twice faster than for other vertical BN composites with the similar thickness reported in other works.[50] As expected, the BN-PVP composites with the horizontal microstructure showed the slowest increase in surface temperature, with an initial speed of about 1 °C s^{-1} only. Also, the temperature after 10 s was about 15 °C lower than the vertically aligned composites. The graded composites exhibited an intermediate heat dissipation between that of the vertical and horizontal composites. Interestingly, the orientation of the samples, V→H or H→V, led to distinct temperature responses. In the case of H→V, the composite exhibited slower temperature

increase in the initial stage as compared to the vertical ones but reached the same temperature profile after 10 s. On the contrary, in the case of V→H, the composite had a lower surface temperature during the overall process (**Figure 5c**). This indicates that the heat dissipation throughout the thickness of the composites is hindered by the horizontal alignment at the top, which likely restricts the heat dissipated along the horizontal plane.

In the second set of experiments, we studied the cooling of the composites after preheating them to about 100 °C and placing them onto a cool substrate (**Figure 5d**, **Figure S7**). As anticipated, the vertically aligned composites exhibited the fastest cooling speed with the same middle band along the plane of alignment of the microplatelet as observed during the heating. The initial cooling speed was of about 12 °C s^{-1}, with a surface temperature decreasing from about 100 °C to less than 40 °C in only 5s, demonstrating efficient heat dissipation (**Figure 5e**). On the contrary, the horizontally aligned composite exhibited the slowest cooling speed about 8 °C s^{-1} in the initial stage. The graded composite again showed different temperature responses depending on the testing configuration. The case V→H showed faster cooling than the other case H→V, which can be attributed to the vertical alignment in contact with the cold substrate enabling rapid heat transfer. After 15s, all composites reached the room temperature. These experiments confirm that the heat transport is the highest along the basal plane of alignment of the BN microplatelets and that microstructural control impacts the thermal response.

We now envision the case where two electronic components or heat sources are stacked above each other, as found in 3D electronics. In this case, heat dissipation through the thickness of a material sandwiched between the two electronic components would not be desirable. A better proposition would be to purposely direct the heat to the side, where a heat sink could be placed to dissipate the heat out of the integrated system. To direct the heat from both the top and bottom surfaces to the side, a graded microstructure as illustrated in **Figure 5g** would be preferred. In this configuration, the heat generated by the two electronic components would be transferred to the right side of the composite following the orientation of the microplatelets. Indeed, heat coming from both top and bottom surfaces would be rapidly conducted inwards the composite through the vertical layers. Then, inclined microplatelets orientation would channel the heat to the right side. Finally, the horizontal layer in the middle would prevent heat from being transferred through the thickness of this layer. Using finite element (FE) analysis, we simulated the temperature distribution within the layered composite (**Figure 5h**, **Figure S8;** see SI and supplementary video for details on the FE simulations). Colour maps of the temperature distribution support anticipated thermal transfer as discussed earlier, with the heat being dissipated to the right following the inclination of the BN in the microstructure.

Furthermore, due to the absence of a heat sink on the right of the composites, and due to the finite geometrical dimension, the middle horizontal layer was found to heat up at the initial stage, resulting in a heat band at the center of the microstructure. The simulation therefore confirms the unique possibility to design inclined fast conductive path for heat transfer to selected areas in the composite. Producing the same desired microstructure using MASC, the temperature distribution through the thickness was recorded using an infrared camera after being placed in contact with two heat sources (**Figure 5i-l**). Right after contact with the heat sources, the temperature increased in the vertical layers of the microstructured BN-PVP composite. Slightly inclined temperature slopes can also be observed in the temperature profile (**Figure 5i**). In the middle of the composite, where the BN microplatelets are horizontally aligned, a higher temperature is also visible, similar to the FE simulation (**Figure 5i** and **5j**). With time, the composite heated up, making the directed heat conduction through the inclined slopes more visible with a symmetric high-temperature pattern in a "V" shape (**Figure 5k**), before reaching the ultimate uniform temperature (**Figure 5l**). If a heat sink was to be placed on the right side of the composite, the heat would have been conducted away preventing heat accumulation in the composite. This proof-of-concept composite therefore demonstrates the capability of our approach to conduct the heat effectively toward specific areas for better thermal management in unusual complex systems. Other microstructural designs of the BN-PVP composites could be derived to adapt to various situations.

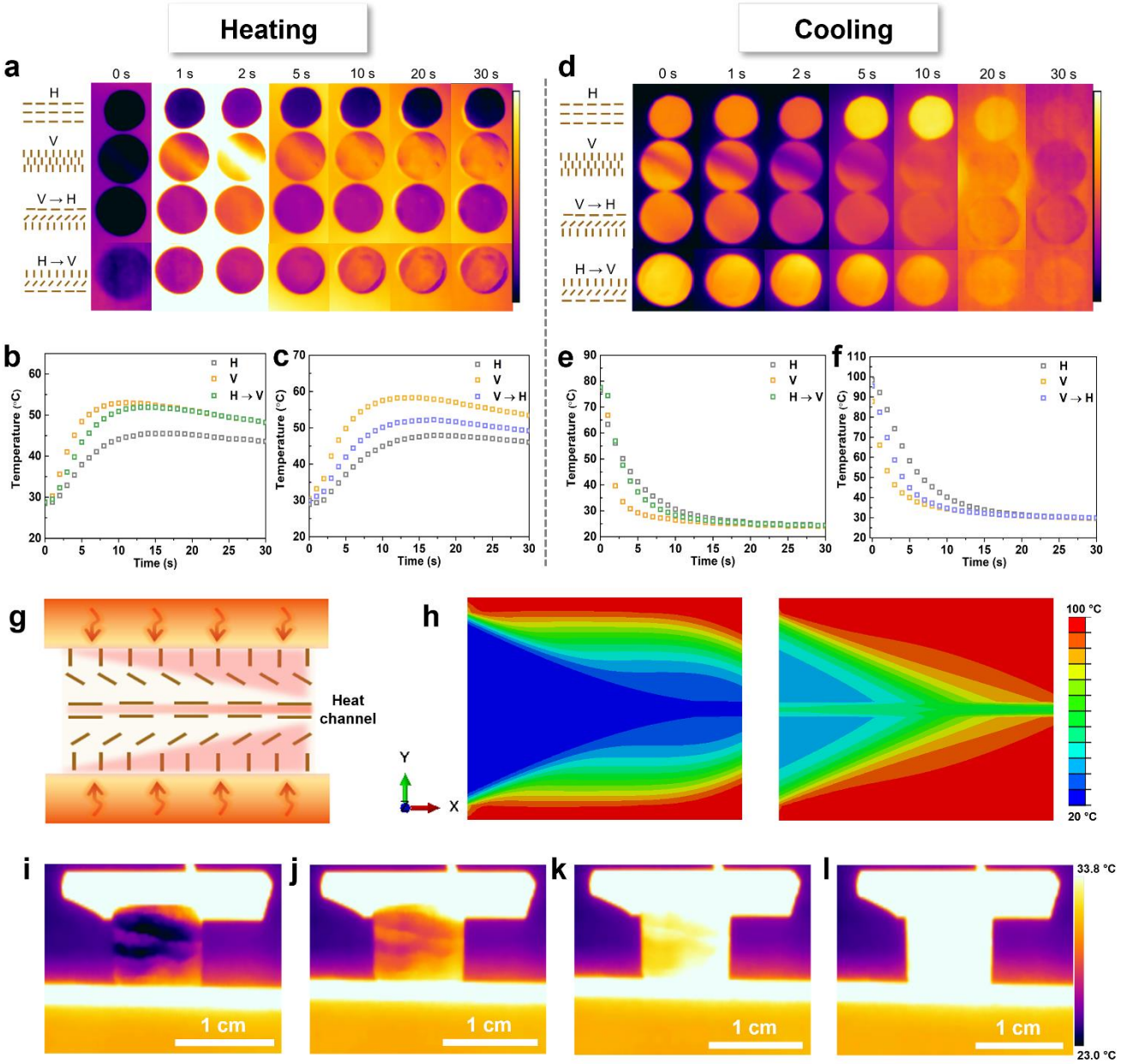

Figure 5. Thermal management capability of BN-PVP composites prepared from the slurry containing 40 wt% m-BN with different local orientation and microstructural design. a) Infrared images recorded during heating showing top surface temperature of the composites of horizontal, vertical, and gradient alignment. The graded composite involves two positionings: one with the horizontal side in contact with the heat source (H→V); another with the vertical side in contact with the heat source (V→H). The surface temperature variations upon heating as a function of time with the graded samples being placed as b) H→V and c) V→H. d) Infrared images recorded during cooling process. The surface temperature of the composites during cooling with graded sample being placed as e) H→V and f) V→H. The contrast of the temperature difference is presented by the colour bar, and the real-time temperature distributions are provided in **Figure S6-7** (SI). g) Schematic illustration showing the microstructural design of the layered composite through its thickness and the formation of directed heat transfer channel (highlighted in pink) when both bottom and top surfaces are in contact with heat sources. h) Simulated temperature distribution of the graded composite with heat coming from top and bottom surfaces using finite element (FE) analysis. i)-l) Infrared images of the side view of the layered composites showing the directional and inclined heat transfer along oriented direction when both surfaces were simultaneously heated.

3. Conclusion

In summary, we demonstrated that BN composites of unusually high thermal conductivity up to 12.1 W m^{-1} K^{-1} along the plane of the BN microplatelets could be obtained by optimizing interplatelet packing and alignment. We also showed that tailoring the local microplatelet orientations in 3D composites could efficiently channel the heat into specific directions. To realize this, we used the technique of MASC where raw crystalline BN platelets are functionalized with a small concentration of iron oxide and assembled into packed and percolating assemblies with high-level of local orientation control using an external magnetic field. Optimization of the slurry composition permitted to find that 40 wt% BN yielded the highest alignment resulting in the outstanding thermal conductivity. Such high thermal conductivity can mainly be attributed to the large lateral size of BN platelets used here, that lowered the interfacial thermal resistance between individual particles, also the high orientation level and the high concentration in BN platelets that guaranteed close platelet packing and continuous thermal paths. In addition, the composites had a low density, a high relative solid loading in BN of about 62.6 vol% leading to a high modulus of 442.3 MPa, a low dielectric constant of 4.9, and electrical insulation. These properties make our BN-PVP composites promising for "traditional" TIM where heat is transferred unidirectionally from a heat source to a heat sink. Finally, another unusual feature of our material lies in the capability to design the microstructure to channel the heat towards specific directions. Graded microstructures were produced to showcase how the heat from two heat sources could be driven to a specific area using this method. Our experimental results were also supported by FE simulations. Overall, microstructured TIMs with tailored heat conduction paths could open up solutions for next-generation thermal management in 3D electronics with high power density.

4. Experimental Section

Materials: Hexagonal boron nitride microplatelets of average diameter 45 μm and thickness 1.1 μm were provided by Momentive. Ferrofluid EMG 605 containing cationic SPIONs was purchased from Ferrotec. Polyvinylpyrrolidone polymer (PVP, MW = 360'000) was purchased from Sigma-Aldrich. Sodium hydroxide was purchased from Sigma-Aldrich and dissolved into 1M solution in water. An ammonium salt of polymethacrylic acid (Dolapix CE 64, Zschimeer & Schwarz, Germany) was selected as the dispersant.

Slurry preparation: First, magnetically responsive BN microplatelets were prepared using the following steps. In a typical process, BN powder (15 g) was dispersed in deionized water (1500 ml) using a magnetic stirrer. The pH of the suspension was adjusted to 10.5 using a solution of NaOH. Then, the ferrofluid EMG 605 solution (1200 μl) was pre-diluted in

deionized water (200 ml) before being added to the BN suspension in a dropwise fashion. The suspension was magnetically stirred at room temperature for 5 days to ensure complete saturated adsorption of the SPIONs from the ferrofluid onto the BN microplatelets. The obtained magnetized BN (m-BN) microplatelets were then filtered and rinsed with deionized water and ethanol, and fully dried at 45 °C. This magnetization of BN microplatelets can be easily upscaled by multiplying the amount of raw materials accordingly.

The new m-BN microplatelets were then used to prepare the slurry. Typically, PVP (0.3 g) was initially dissolved in deionized water (3.6 g), followed by the addition of Dolapix (0.05 g) to assist dispersion of the microplatelets. Once the PVP solution was obtained, the appropriate amount of m-BN powder was introduced at 20 wt%, 30 wt%, 40 wt%, 45 wt%, and 50 wt%. The slurry was further homogenized and degassed by repeatedly applying vortex mixing, planetary centrifugal mixing, and magnetically stirring.

Magnetically assisted slip casting of microstructured BN composites: Prior to the casting, porous gypsum substrates were prepared by mixing gypsum powder (Ceramix, Germany) with deionized water and casting them in flat molds. The gypsum substrates were fully dried before use. To prepare the oriented composites, the as-prepared slurry was poured into a cylindric mold placed on the flat gypsum substrate, under a magnetic field rotating at a frequency of 1 Hz. The magnetic field was generated from a neodymium magnet (3 cm x 1 cm, Eclipse, Singapore) attached to a rotating motor (238-9715, RS PRO, Singapore) and the mold was placed so that the magnetic field covering the area of the sample had a strength between 30 to 50 mT. The filler orientation in the slurry can be easily tuned by changing the rotation direction of the magnet to prepare composites with vertical, horizontal, graded, or other complex alignment patterns. After complete water removal from the slurry through the pores of the gypsum substrate, the consolidated composite was thoroughly dried at 45 °C. To make comparisons, the randomly aligned composites were prepared by slip casting without applying any magnetic field.

Characterization: The surface coating and EDS mapping of the m-BN microplatelets was observed using field emission scanning electron microscopy (FESEM, JEOL JSM-6340F, Japan). The microstructures of the as-prepared m-BN-PVP composites were observed by scanning electron microscopy (SEM, JEOL JSM-5600LV, Japan) on fractured cross-sections. The surfaces of the samples were sputtered with a thin layer of gold before observation. The m-BN microplatelets alignment in the composites was further characterized using the Fast-Fourier Transform (FFT) patterns derived from SEM images of a 500 times magnification by image processing in the software Image J (see SI for more details). The gray value curve as a function of pixels was generated along the major and minor axes of the ellipse of the FFT, and the

corresponding Full Width at Half Maximum (FWHM) values were obtained from the Gaussian fitting curve. The crystallographic phases and orientation degree in the composites were characterized using an X-ray diffractometer (XRD, Shimadzu XRD-6000, Japan) with Cu Kα radiation (λ = 1.54056 Å). A continuous scan mode with a step degree of 0.02° and a scan speed of 2.0 degree per minute was utilized in the range from 20 to 80°. The viscosity of the slurries was characterized using a rheometer (Bohlin, Malvern Instruments, UK) with serrated parallel plate. Thermogravimetric analysis (TGA, TA instruments, Q500, Germany) and differential scanning calorimetry (DSC, TA instruments, Q2000) analysis were performed in N_2 at a rate of 15 °C per minute. Before conducting thermal conductivity characterization, the top and bottom surfaces of the composites were made parallel by grinding. The samples were prepared in cylindrical shape with a diameter of 12.7 mm, a thickness about 2 mm, and coated with a thin layer of graphite spray on both top and bottom surfaces. A laser flash apparatus (TA instruments, DLF 1200, Germany) was used to measure the thermal diffusivity α, and the heat capacity $C_p$of composites. The through-thickness thermal conductivity, K, was then calculated using:

$$K = \rho \alpha C_p \qquad (3)$$

where ρ is the density measured by Archimedes method in silicone oil. Compression tests were carried out using a Universal testing system (Instron 3366, USA) with a load cell of 500 N, on cylindrical samples with a diameter about 4.5 mm and a height about 6 mm. Each alignment type involved 5 specimens for fabrication and testing. The Vickers hardness was measured using a microindenter (Future-Tech microhardness tester, FM-300e) and the geometry of the indents was observed using an optical microscopy (Olympus, SZX 16, Japan). The indentation procedures were repeated 5 times for each sample. The electrical resistivity was measured using a four-point probe system (Advanced Instrument Technology, CMT-SR2000N, USA). Dielectric properties of the composites were measured using an impedance analyzer system (Solartron Ametek, 1296A Dielectric Interface, USA) with both surfaces coated with a thin layer of silver paste. The infrared thermal images of the composites were recorded using thermal imaging system and repeated at least 5 times for each process (FLIR, ETS320, USA). The emissivity parameter was calibrated before temperature recording, and a fixed emissivity of 0.95 was applied for all composites. The samples with different alignment were prepared in cylindrical shape with a diameter about 8.6 mm and a thickness of 1.5 mm. For heating process, an alumina substrate was preheated to 100 °C and placed under the infrared camera as heating source. Then the composite samples were simultaneously transferred on the preheated substrate for temperature recording. For cooling process, the samples were heated to 100 °C and immediately transferred to a cool alumina substrate at the ambient temperature of 25 °C. In

observation of directional heat transfer, the graded composite was prepared in cylindrical shape with a diameter of 8.6 mm and thickness of 6 mm. Then, both top and bottom surfaces of the sample were simultaneously heated by a preheated silicon wafer and a hot plate, respectively, at the temperature of 50 °C.

Supporting Information

Supporting Information is available from the Wiley Online Library or from the author.

Acknowledgements

The authors acknowledge funding from Nanyang Technological University of Singapore (Start-Up grant) and from the National Research Foundation of Singapore (award NRF-NRFF12-2020-0002).

Conflict of Interest

The authors declare no conflict of interest.

Data availability

The data that support the findings of this study are available from the corresponding author on request.

References

[1] R. J. McGlen, R. Jachuck, S. Lin, *Appl. Therm. Eng.* **2004**, 24, 1143.
[2] A. Bar-Cohen, P. Wang, *J. Heat Transfer* **2012**, 134.
[3] M. M. Waldrop, *Nature News* **2016**, 530, 144.
[4] A. L. Moore, L. Shi, *Mater. Today* **2014**, 17, 163.
[5] M. Loeblein, S. H. Tsang, M. Pawlik, E. J. R. Phua, H. Yong, X. W. Zhang, C. L. Gan, E. H. T. Teo, *ACS nano* **2017**, 11, 2033.
[6] J. Ma, T. Shang, L. Ren, Y. Yao, T. Zhang, J. Xie, B. Zhang, X. Zeng, R. Sun, J.-B. Xu, *Chem. Eng. J* **2020**, 380, 122550.
[7] J. Due, A. J. Robinson, *Appl. Therm. Eng.* **2013**, 50, 455.
[8] V. Venkatadri, B. Sammakia, K. Srihari, D. Santos, **2011**.
[9] R. Li, X. Yang, J. Li, Y. Shen, L. Zhang, R. Lu, C. Wang, X. Zheng, H. Chen, T. Zhang, *Mater. Today Phys.* **2021**, 100594.
[10] I. Jo, M. T. Pettes, J. Kim, K. Watanabe, T. Taniguchi, Z. Yao, L. Shi, *Nano letters* **2013**, 13, 550.
[11] H. Shen, J. Guo, H. Wang, N. Zhao, J. Xu, *ACS Appl. Mater. interfaces* **2015**, 7, 5701.
[12] K. Sato, H. Horibe, T. Shirai, Y. Hotta, H. Nakano, H. Nagai, K. Mitsuishi, K. Watari, *J. Mater. Chem.* **2010**, 20, 2749.
[13] L. Lindsay, D. Broido, *Phys. Rev. B* **2011**, 84, 155421.
[14] Q. Song, W. Zhu, Y. Deng, F. Hai, Y. Wang, Z. Guo, *Compos. Part A Appl. Sci. Manuf.* **2019**, 127, 105654.
[15] Z. Wang, J. Huang, S. Chen, M. Yang, J. Liu, Q. Xie, Y. Cheng, presented at *2017 IEEE*

International Workshop On Integrated Power Packaging (IWIPP), **2017**.
[16] J. Hu, Y. Huang, X. Zeng, Q. Li, L. Ren, R. Sun, J.-B. Xu, C.-P. Wong, *Compos. Sci. Technol.* **2018**, 160, 127.
[17] J. Liu, W. Li, Y. Guo, H. Zhang, Z. Zhang, *Compos. Part A Appl. Sci. Manuf.* **2019**, 120, 140.
[18] J. Hu, Y. Huang, Y. Yao, G. Pan, J. Sun, X. Zeng, R. Sun, J.-B. Xu, B. Song, C.-P. Wong, *ACS Appl. Mater. interfaces* **2017**, 9, 13544.
[19] B. Ghosh, F. Xu, D. M. Grant, P. Giangrande, C. Gerada, M. W. George, X. Hou, *Adv. Electron. Mater.* **2020**, 6, 2000627.
[20] Z. Lin, Y. Liu, S. Raghavan, K.-s. Moon, S. K. Sitaraman, C.-p. Wong, *ACS Appl. Mater. Interfaces* **2013**, 5, 7633.
[21] C. Yuan, B. Duan, L. Li, B. Xie, M. Huang, X. Luo, *ACS Appl. Mater. Interfaces* **2015**, 7, 13000.
[22] A. Gurijala, R. B. Zando, J. L. Faust, J. R. Barber, L. Zhang, R. M. Erb, *Matter* **2020**, 2, 1015.
[23] H. Le Ferrand, *J. Eur. Ceram. Soc.* **2021**, 41, 24.
[24] H. Le Ferrand, F. Bouville, T. P. Niebel, A. R. Studart, *Nat. Mater.* **2015**, 14, 1172.
[25] H. Le Ferrand, F. Bouville, A. R. Studart, *Soft Matter* **2019**, 15, 3886.
[26] X. Y. Chan, C. Chua, S. Tan, H. Le Ferrand, *Compos. B. Eng.* **2022**, 109608.
[27] C. Zhi, Y. Bando, C. Tan, D. Golberg, *Solid State Commun.* **2005**, 135, 67.
[28] W. S. Khan, N. N. Hamadneh, W. A. Khan, *PLoS One* **2017**, 12, e0183920.
[29] H. S. Lim, J. W. Oh, S. Y. Kim, M.-J. Yoo, S.-D. Park, W. S. Lee, *Chem. Mater.* **2013**, 25, 3315.
[30] C. Chen, Y. Xue, Z. Li, Y. Wen, X. Li, F. Wu, X. Li, D. Shi, Z. Xue, X. Xie, *Chem. Eng. J.* **2019**, 369, 1150.
[31] K. Kim, J. Kim, *Int. J. Therm. Sci.* **2016**, 100, 29.
[32] X. Jia, Q. Li, C. Ao, R. Hu, T. Xia, Z. Xue, Q. Wang, X. Deng, W. Zhang, C. Lu, *Compos. Part A Appl. Sci. Manuf.* **2020**, 129, 105710.
[33] F. Jiang, N. Song, R. Ouyang, P. Ding, *ACS Appl. Mater. Interfaces* **2021**, 13, 7556.
[34] R. Wang, H. Cheng, Y. Gong, F. Wang, X. Ding, R. Hu, X. Zhang, J. He, X. Tian, *ACS Appl. Mater. Interfaces* **2019**, 11, 42818.
[35] L. Ren, X. Zeng, R. Sun, J.-B. Xu, C.-P. Wong, *Chem. Eng. J.* **2019**, 370, 166.
[36] W. Yan, Y. Zhang, H. Sun, S. Liu, Z. Chi, X. Chen, J. Xu, *J. Mater. Chem. A* **2014**, 2, 20958.
[37] X. Chen, J. S. K. Lim, W. Yan, F. Guo, Y. N. Liang, H. Chen, A. Lambourne, X. Hu, *ACS Appl. Mater. Interfaces* **2020**, 12, 16987.
[38] J. Yang, L.-S. Tang, R.-Y. Bao, L. Bai, Z.-Y. Liu, W. Yang, B.-H. Xie, M.-B. Yang, *Chem. Eng. J.* **2017**, 315, 481.
[39] J. Yang, L.-S. Tang, R.-Y. Bao, L. Bai, Z.-Y. Liu, W. Yang, B.-H. Xie, M.-B. Yang, *J. Mater. Chem. A* **2016**, 4, 18841.
[40] W. Han, Y. Bai, S. Liu, C. Ge, L. Wang, Z. Ma, Y. Yang, X. Zhang, *Compos. Part A Appl. Sci. Manuf.* **2017**, 102, 218.
[41] J. Chen, X. Huang, Y. Zhu, P. Jiang, *Adv. Funct. Mater.* **2017**, 27, 1604754.
[42] F. Wang, X. Zeng, Y. Yao, R. Sun, J. Xu, C.-P. Wong, *Sci. Rep.* **2016**, 6, 1.
[43] W. Han, M. Chen, W. Song, C. Ge, X. Zhang, *Ceram. Int.* **2020**, 46, 7595.
[44] K. Wu, J. Fang, J. Ma, R. Huang, S. Chai, F. Chen, Q. Fu, *ACS Appl. Mater. Interfaces* **2017**, 9, 30035.
[45] J. Yu, H. Mo, P. Jiang, *Polym. Adv. Technol.* **2015**, 26, 514.
[46] X. Hou, Y. Chen, L. Lv, W. Dai, S. Zhao, Z. Wang, L. Fu, C.-T. Lin, N. Jiang, J. Yu, *ACS Appl. Nano Mater.* **2019**, 2, 360.
[47] Z. Hu, S. Wang, G. Chen, K. Wu, J. Shi, L. Liang, M. Lu, *Compos. Sci. Technol.* **2018**, 168, 287.
[48] K. Wu, J. Wang, D. Liu, C. Lei, D. Liu, W. Lei, Q. Fu, *Adv. Mater.* **2020**, 32, 1906939.
[49] J. Chen, X. Huang, B. Sun, Y. Wang, Y. Zhu, P. Jiang, *ACS Appl. Mater. Interfaces* **2017**, 9, 30909.
[50] J. Han, G. Du, W. Gao, H. Bai, *Adv. Funct. Mater.* **2019**, 29, 1900412.
[51] H. Hong, Y. H. Jung, J. S. Lee, C. Jeong, J. U. Kim, S. Lee, H. Ryu, H. Kim, Z. Ma, T. i. Kim, *Adv. Funct. Mater.* **2019**, 29, 1902575.
[52] S. J. Kang, H. Hong, C. Jeong, J. S. Lee, H. Ryu, J.-h. Yang, J. U. Kim, Y. J. Shin, T.-i. Kim, *Nano Res.* **2021**, 14, 3253.
[53] A. Laturia, M. L. Van de Put, W. G. Vandenberghe, *npj 2D Mater. Appl.* **2018**, 2, 1.

Table of contents entry

Using the magnetically assisted slip casting (MASC) method, the microstructures of boron nitride composites are purposely designed and highly oriented to achieve unusual high thermal conductivity and directional heat transfer towards specific areas along the direction of microplatelets alignment, opening up the solutions for the next-generation thermal management for 3D electronic packaging.

H. He, W. Peng, J. Liu, X. Y. Chan, S. Liu, L. Lu, H. Le Ferrand*

Microstructured BN composites with internally designed high thermal conductivity paths for 3D electronic packaging

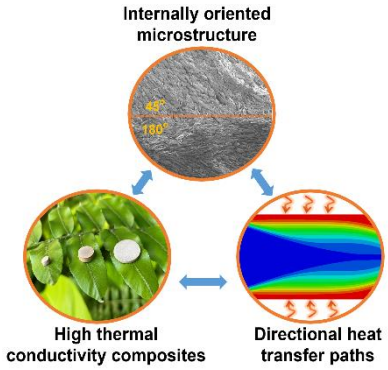

Supporting Information

Microstructured BN composites with internally designed high thermal conductivity paths for 3D electronic packaging

*Hongying He, Weixiang Peng, Junbo Liu, Xin Ying Chan, Shike Liu, Li Lu, and Hortense Le Ferrand**

**Corresponding author: hortense@ntu.edu.sg*

1. Calculation of conformation factor

The conformation factor C_f is applied to quantify the quality of the orientation level using the calculation based on the FFT patterns. The FFT patterns are derived from the cross-sectional SEM images of the composites using the software Image J. All the SEM images utilized were under the same magnification for comparison, typically 500 times in this study. Generally, the shape of the FFT patterns will be near elliptical geometry and can be used as an index for the orientation level of the BN platelets. If the microstructure is in random alignment, the unaligned platelets will contribute to a FFT pattern in circular shape (**Figure S2a**). If the microstructure is highly aligned, the FFT pattern will exhibit a compressed ellipse (**Figure S2b**). The overall direction of platelet orientation is perpendicular to the major axis of the ellipse. After defining the major and minor axis of the ellipse of the FFT patterns, the corresponding gray value curve as a function of pixels can be derived, typically as shown in **Figure S2c**. Using Gaussian fitting, the Full Width at Half Maximum (FWHM) value can be obtained from the gray value curve (**Figure S2d**), and the conformation factor is calculated from the ratio of FWHM values derived along the major axis (F_M) versus the minor axis (F_N).

2. Finite element (FE) simulation method

Finite element (FE) simulation was performed using the software Abaqus 2020 to visualize the directional temperature distribution process during heating. The initial FE model of the layered BN-PVP composite depending on the experimental conditions is depicted in **Figure S8**. The geometrical model is established in the two-dimensional size 6 mm * 6 mm. The layered model includes the top and bottom vertical layers (0.4 mm), the middle horizontal layer (0.4 mm) and the transition layers (2.4 mm) with an orientation angle of 45° to the horizontal layer. The whole

model is meshed into 3600 elements in total with the basic unit of quadrilateral DC2D4 element with the minimum size of 0.1 mm. The whole system is set at room temperature (20 ℃) while the heat source with constant temperature 100 ℃ was applied at the top and bottom boundary to generate the heat flux during heating process. For each oriented layer, the material parameters were set based on experimentally measured values. To illustrate the directional temperature distribution more obviously, a higher thermal conductivity along the platelet alignment direction of 120 W m^{-1} K^{-1} was applied (experimental result as 12.1 W m^{-1} K^{-1}) for higher anisotropy in thermal conduction, and the thermal conductivity perpendicular to the platelet alignment direction of 0.64 W m^{-1} K^{-1} and a specific heat capacity of 645.2 J kg^{-1} K^{-1} were utilized. The video of the temperature distribution process can be found in Supplementary Video.

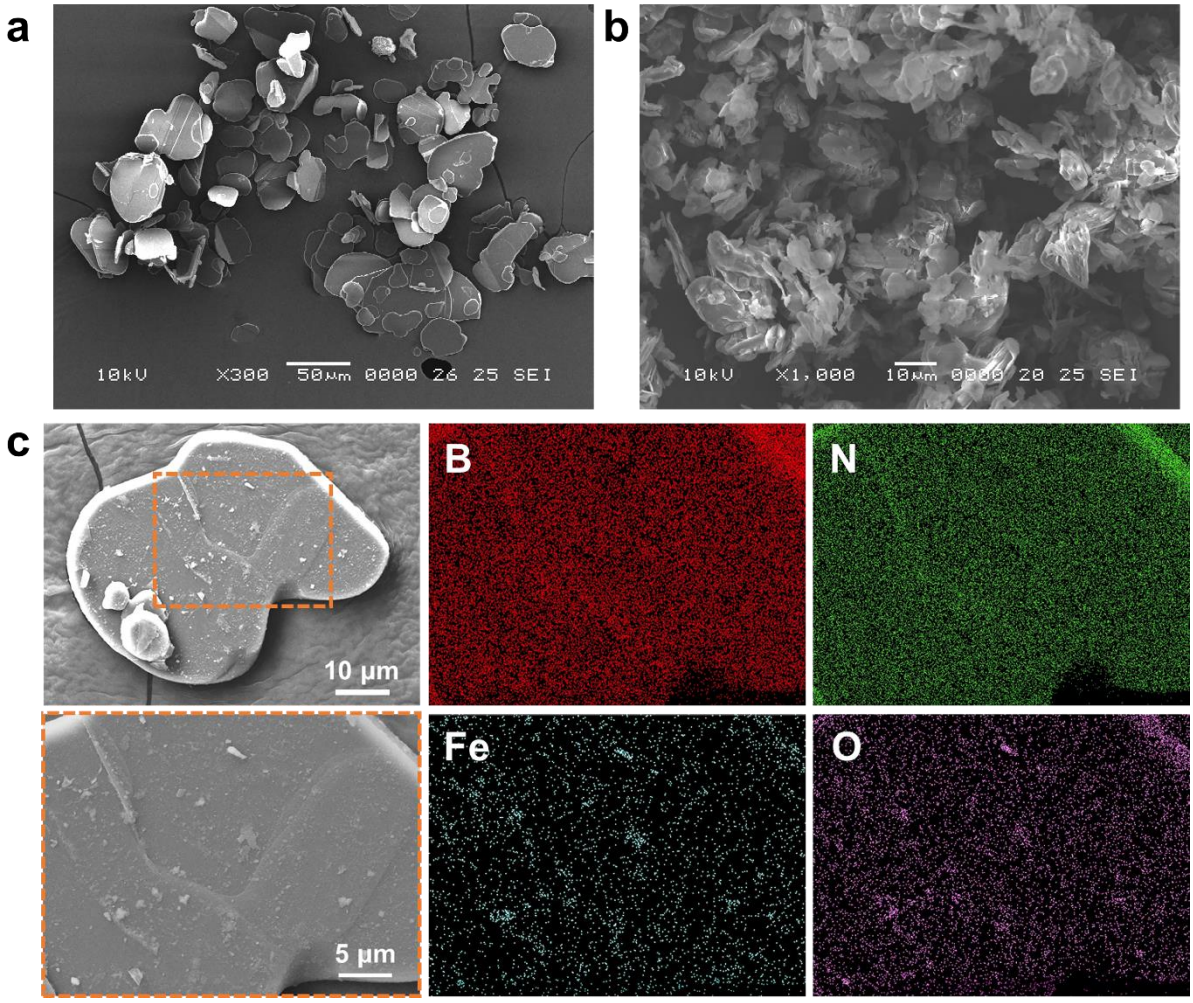

Figure S1. Electron micrographs of raw BN powder with average lateral size of a) 45 µm and b) 9 µm. The BN platelets with large lateral size exhibit negligible aggregation. c) Micrographs and EDS mappings of the surface of a magnetized BN microplatelet showing the coating with iron oxide nanoparticles.

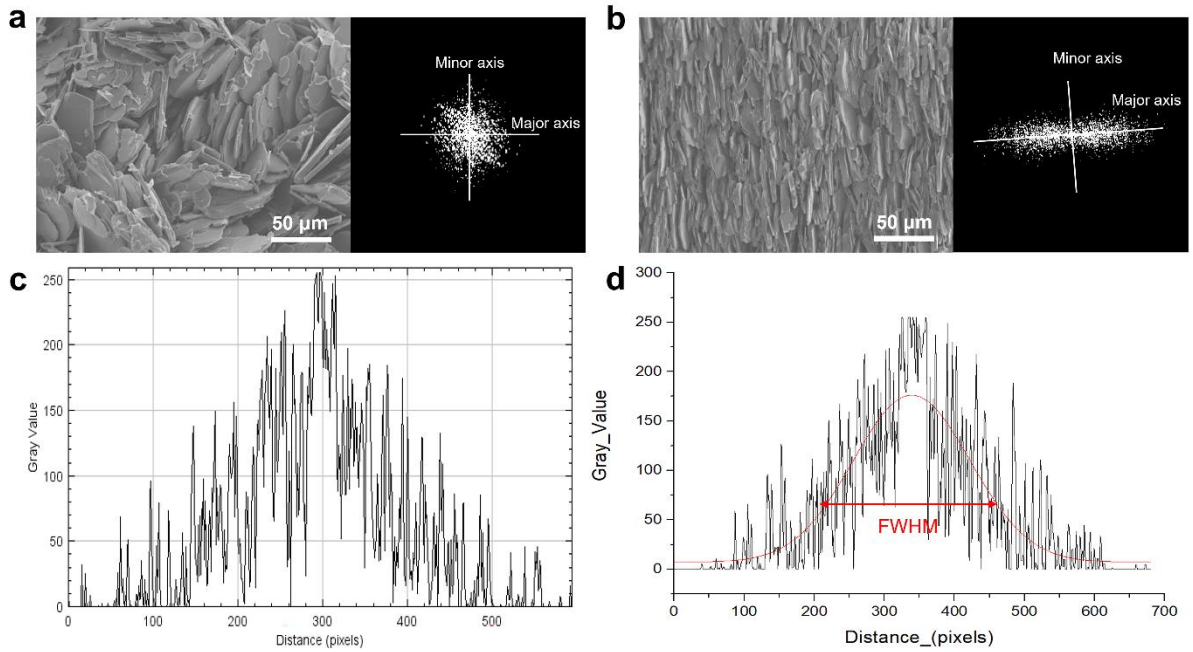

Figure S2. Evaluation of conformation factor from cross-sectional SEM images and derived FFT patterns. a) Typical cross-sectional SEM image and derived FFT pattern of the randomly aligned composite. b) Typical cross-sectional SEM image and derived FFT pattern of the vertically aligned composite. c) Representative gray value curve as a function of pixels derived from selected axis of FFT pattern. d) The FWHM value obtained from Gaussian fitting of the gray value curve.

Figure S3. The color difference of BN-PVP composites with different oriented microstructures prepared by MASC.

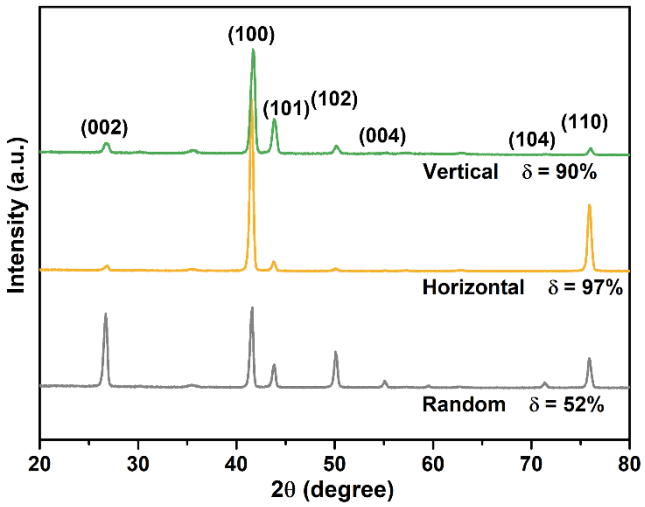

Figure S4. XRD pattens and calculated degree of orientation δ of composites in vertical, horizontal, and random alignment.

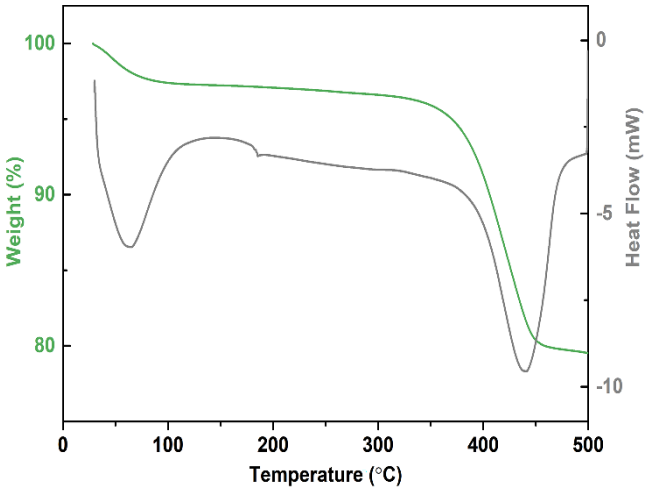

Figure S5. TGA and DSC results of 40 wt% BN-PVP composite in the temperature range up to 500 °C.

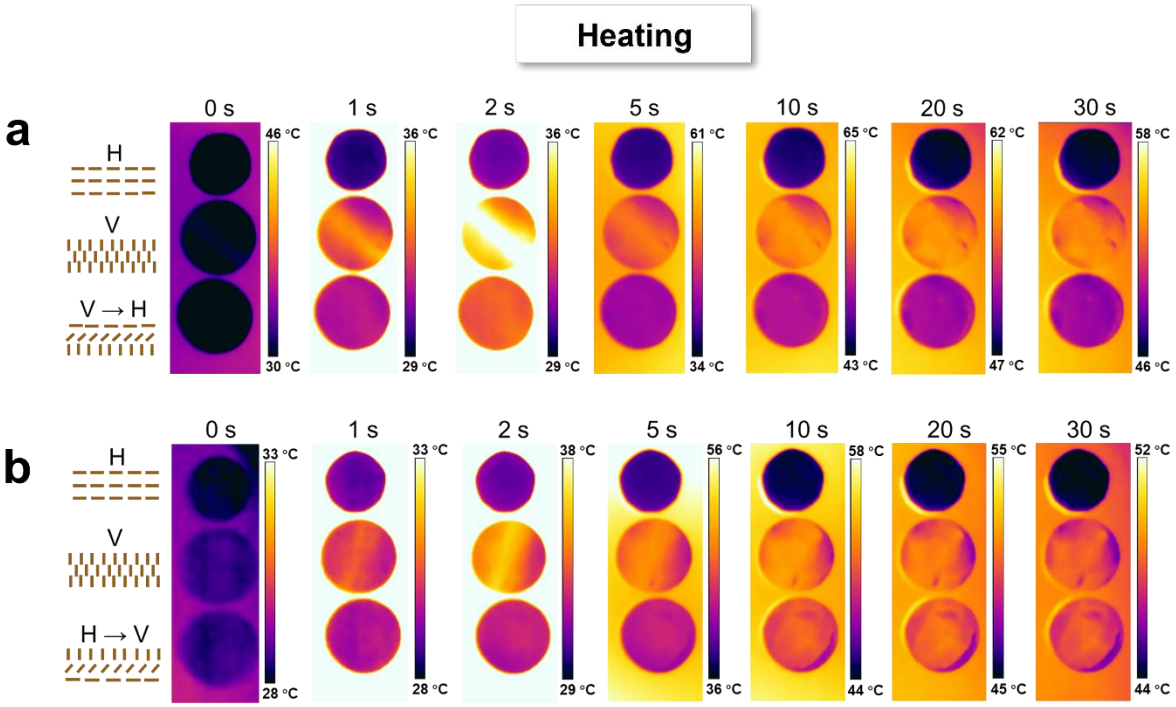

Figure S6. The real-time temperature distribution of composite top surfaces during heating.

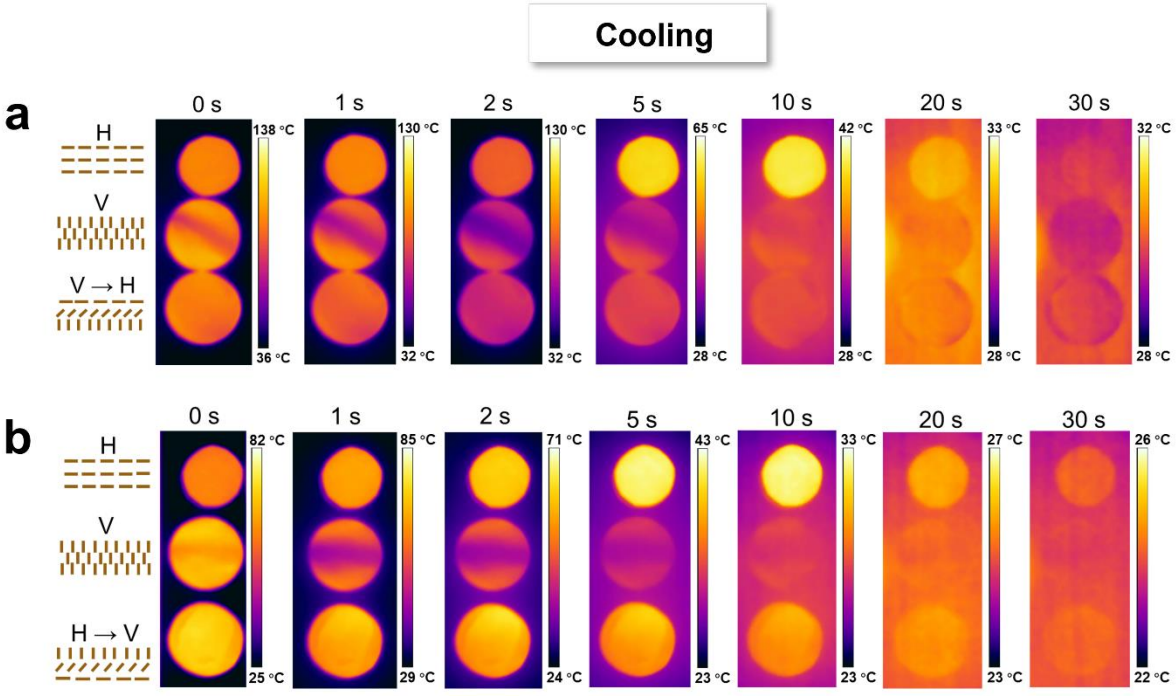

Figure S7. The real-time temperature distribution of composite top surfaces during cooling.

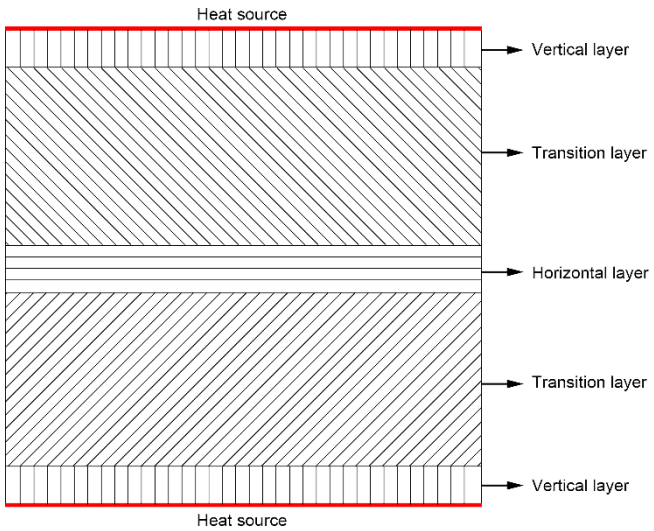

Figure S8. Schematic diagram of BN-PVP composites for FE simulation.

Table S1. Through-thickness thermal conductivity of BN-based and exfoliated BNNS-based composites reported in literature and this work. The volume concentration of the composites labelled with asterisk symbol were estimated and converted from wt% to vol% using the reported density of fillers and matrix.

Material composition	Filler concentration	Through-thickness thermal conductivity ($W\ m^{-1}\ K^{-1}$)	Ref.
BN-based composite			
BN-PVP	62.6 vol%	12.1	This work
BN-Silicone	9.14 vol%	0.58	2015 [1]
BN-Epoxy	20 vol%	4.7	2013 [2]
BN-Epoxy*	20 wt% (~12.5 vol%)	0.85	2013 [3]
BN-Epoxy*	20 wt% (~11.8 vol%)	0.79	2019 [4]
BN-Epoxy	60 vol%	8.67	2020 [5]
BN-Epoxy	30 vol%	3.45	2016 [6]
BN-CS-PEG*	27 wt% (~16.5 vol%)	2.77	2020 [7]
BN-PEG	8.1 vol%	1.3	2021 [8]
BN-PS*	33.3 wt% (~18.96 vol%)	0.94	2019 [9]
BN-PDMS*	50 wt% (~31.5 vol%)	2.3	2019 [10]
BN-cMWCNTs-PI*	3 wt% (~2 vol%)	0.39	2014 [11]
BN-Epoxy-PVDF*	21 wt% (~12.2 vol%)	1.23	2020 [12]
BN-Graphene-PEG*	30 wt% (~17.5 vol%)	1.33	2017 [13]
BN-GO-PEG*	19.2 wt% (~11.3 vol%)	1.84	2016 [14]
BN-PS-CPS*	15.9 wt% (~11.23 vol%)	0.69	2017 [15]
BNNS-based composite			
BNNS-Epoxy-AgNps*	20 wt% (~10.89 vol%)	1.13	2019 [4]
BNNS-Epoxy	9.6 vol%	3.13	2016 [16]
BNNS-AgNPs-Epoxy	25.1 vol%	3.05	2016 [17]
BNNS-PS*	12 wt% (~6.08 vol%)	1.13	2020 [18]
BNNS-CNF*	70 wt% (~64 vol%)	0.8	2017 [19]
BNNS-Epoxy-HBP	50 vol%	9.81	2015 [20]
BNNS-CS-PDMS	15.8 vol%	7.46	2019 [21]
BNNS-CNF*	25 wt% (~20.24 vol%)	1.1	2018 [22]

BNNS-ANF*	45 wt% (~35.9 vol%)	0.19	2020 [23]
BNNS-PDMS-PVA	15.6 vol%	1.94	2017 [24]

Table S2. Measured density, thermal diffusivity, and heat capacity of BN-PVP composites with various filler concentration and orientation microstructures of vertical (V), horizontal (H), and random (R) at room temperature.

BN composition	Density ($g\ cm^{-3}$)	Thermal diffusivity ($mm^2\ s^{-1}$)	Heat capacity ($J\ kg^{-1}\ K^{-1}$)
20 wt%-V	1.0	3.7	589.1
30 wt%-V	1.6	5.2	351.3
40 wt%-V	1.3	14.1	645.2
40 wt%-H	1.1	0.8	795.6
40 wt%-R	1.1	2.1	742.7
45 wt%-V	1.3	5.8	675.0
50 wt%-V	1.0	6.1	598.5

References

[1] C. Yuan, B. Duan, L. Li, B. Xie, M. Huang, X. Luo, *ACS Appl. Mater. Interfaces* **2015**, 7, 13000.
[2] H. S. Lim, J. W. Oh, S. Y. Kim, M.-J. Yoo, S.-D. Park, W. S. Lee, *Chem. Mater.* **2013**, 25, 3315.
[3] Z. Lin, Y. Liu, S. Raghavan, K.-s. Moon, S. K. Sitaraman, C.-p. Wong, *ACS Appl. Mater. Interfaces* **2013**, 5, 7633.
[4] C. Chen, Y. Xue, Z. Li, Y. Wen, X. Li, F. Wu, X. Li, D. Shi, Z. Xue, X. Xie, *Chem. Eng. J.* **2019**, 369, 1150.
[5] A. Gurijala, R. B. Zando, J. L. Faust, J. R. Barber, L. Zhang, R. M. Erb, *Matter* **2020**, 2, 1015.
[6] K. Kim, J. Kim, *Int. J. Therm. Sci.* **2016**, 100, 29.
[7] X. Jia, Q. Li, C. Ao, R. Hu, T. Xia, Z. Xue, Q. Wang, X. Deng, W. Zhang, C. Lu, *Compos. Part A Appl. Sci. Manuf.* **2020**, 129, 105710.
[8] F. Jiang, N. Song, R. Ouyang, P. Ding, *ACS Appl. Mater. Interfaces* **2021**, 13, 7556.
[9] R. Wang, H. Cheng, Y. Gong, F. Wang, X. Ding, R. Hu, X. Zhang, J. He, X. Tian, *ACS Appl. Mater. Interfaces* **2019**, 11, 42818.
[10] L. Ren, X. Zeng, R. Sun, J.-B. Xu, C.-P. Wong, *Chem. Eng. J.* **2019**, 370, 166.
[11] W. Yan, Y. Zhang, H. Sun, S. Liu, Z. Chi, X. Chen, J. Xu, *J. Mater. Chem. A* **2014**, 2, 20958.
[12] X. Chen, J. S. K. Lim, W. Yan, F. Guo, Y. N. Liang, H. Chen, A. Lambourne, X. Hu, *ACS Appl. Mater. Interfaces* **2020**, 12, 16987.
[13] J. Yang, L.-S. Tang, R.-Y. Bao, L. Bai, Z.-Y. Liu, W. Yang, B.-H. Xie, M.-B. Yang, *Chem. Eng. J.* **2017**, 315, 481.
[14] J. Yang, L.-S. Tang, R.-Y. Bao, L. Bai, Z.-Y. Liu, W. Yang, B.-H. Xie, M.-B. Yang, *J. Mater. Chem. A* **2016**, 4, 18841.
[15] W. Han, Y. Bai, S. Liu, C. Ge, L. Wang, Z. Ma, Y. Yang, X. Zhang, *Compos. Part A Appl. Sci. Manuf.* **2017**, 102, 218.
[16] J. Chen, X. Huang, Y. Zhu, P. Jiang, *Adv. Funct. Mater.* **2017**, 27, 1604754.
[17] F. Wang, X. Zeng, Y. Yao, R. Sun, J. Xu, C.-P. Wong, *Sci. Rep.* **2016**, 6, 1.
[18] W. Han, M. Chen, W. Song, C. Ge, X. Zhang, *Ceram. Int.* **2020**, 46, 7595.
[19] K. Wu, J. Fang, J. Ma, R. Huang, S. Chai, F. Chen, Q. Fu, *ACS Appl. Mater. Interfaces* **2017**, 9, 30035.
[20] J. Yu, H. Mo, P. Jiang, *Polym. Adv. Technol.* **2015**, 26, 514.
[21] X. Hou, Y. Chen, L. Lv, W. Dai, S. Zhao, Z. Wang, L. Fu, C.-T. Lin, N. Jiang, J. Yu, *ACS Appl. Nano Mater.* **2019**, 2, 360.
[22] Z. Hu, S. Wang, G. Chen, K. Wu, J. Shi, L. Liang, M. Lu, *Compos. Sci. Technol.* **2018**, 168, 287.
[23] K. Wu, J. Wang, D. Liu, C. Lei, D. Liu, W. Lei, Q. Fu, *Adv. Mater.* **2020**, 32, 1906939.
[24] J. Chen, X. Huang, B. Sun, Y. Wang, Y. Zhu, P. Jiang, *ACS Appl. Mater. Interfaces* **2017**, 9, 30909.